



Genesis Mechanism of Heat Source in Mianhuakeng Uranium Deposit, South China: Insights from Radiogenic Heat Production of Granite Bodies

WANG Siqi¹, ZHANG Baojian^{1,2,*}, LÜ Guosen^{3,4}, LIU Feng³ and ZHU Xi³

¹ Chinese Academy of Geological Sciences, Beijing 100037, China

² Technology Innovation Center for Carbon Sequestration and Geological Energy Storage, Ministry of Natural Resources, Beijing 100037, China

³ Institute of Hydrogeology and Environmental Geology, Chinese Academy of Geological Sciences, Shijiazhuang 050061, China

⁴ China University of Geosciences, Wuhan 430074, China

Abstract: The Mianhuakeng uranium deposit, characterized by uranium-rich granite, serves as a key site for research into crustal radioactive heating. Based on 45 rock samples, this study reviews that the host granite in the Mianhuakeng uranium deposit has a high radioactive heat production rate (avg. 5.50 $\mu\text{W}/\text{m}^3$) and a low Th/U ratio (avg. 2.62). Uranium-rich granite and its alteration zone within the upper crust (0–5 km depth) contribute about 45% of the total radioactive heat production, which is crucial for controlling geothermal resource distribution. For uranium-thermal at tectonic plate margins, a symbiotic geological model was proposed: Firstly, subduction of the Pacific Plate caused upwelling of the asthenosphere, generating a high heat-flow background. Secondly, heat transfer is enhanced by major faults such as the Youdong and Mianhuakeng faults. Subsequently, uranium was mobilized, transported, and enriched within the granite through deep siliceous hydrothermal activity and associated alteration. Ultimately, the uranium enrichment in granite leads to increased radioactive heat production, resulting in local thermal anomalies. This model provides a theoretical support for exploring and developing uranium-thermal symbiotic resources in South China.

Key words: uranium-rich granite, radiogenic heat production, heat source, genesis mechanism, Mianhuakeng uranium deposit

Citation: Wang et al., 2026. Genesis Mechanism of Heat Source in Mianhuakeng Uranium Deposit, South China: Insights from Radiogenic Heat Production of Granite Bodies. *Acta Geologica Sinica (English Edition)*, 100(1): 286–296. DOI: 10.1111/1755-6724.70036

1 Introduction

Terrestrial heat flow and radioactive heat production significantly influence the formation mechanisms of geothermal resources, attracting considerable research interest (Mareschal and Jaupart, 2013; Artemieva et al., 2017; Zhou et al., 2020). Terrestrial heat flow is the most direct surface indicator of the Earth's interior thermal state. It comprises two main components: heat generated by the radioactive decay of elements within crustal rocks, primarily uranium (U), thorium (Th), and potassium (K), and heat originating from the mantle (Furlong et al., 2013; Erbek and Dolmaz, 2019; Jiang et al., 2019). Understanding the distribution of heat flow, which controls the distribution of deep geothermal fields and the thermodynamic processes within the crust and mantle, represents a major advance in geothermal research. Within this framework, the radioactive heat produced by rocks is a key parameter (Kremenetsky et al., 1989; Abbady and Al-Ghamdi, 2018). Therefore, quantifying the radioactive

heat production of rocks is essential for elucidating the heat source mechanisms in geothermal anomaly regions.

South China constitutes a major region of mineral and geothermal riches in China, with considerable potential for geothermal resource development. Heat conduction inside the mantle, radioactive heat production from granite in the crust, and a low-velocity body of the middle and lower crust in some locations are the main heat sources in the Fujian–Guangdong–Hainan region (Zheng et al., 2021; Zheng and Luo, 2024; Yang et al., 2025). Among them, the heat production rate of granite typically ranges from 2 to 10 $\mu\text{W}/\text{m}^3$, with more than 50% of analyzed samples falling within the 4 and 7 $\mu\text{W}/\text{m}^3$ (Wan et al., 2015; Kuang et al., 2020; Zhou et al., 2020). Moreover, these granites are closely associated with a variety of metal deposits, such as uranium, and geothermal anomalies, like hot springs (Yang et al., 2016). Collectively, these observations highlight the substantial research potential of the radioactive heat production from granites in this region.

* Corresponding author. E-mail: zbjssdk@126.com

The Mianhuakeng uranium deposit was discovered during the 1950s within the Zhuguangshan granitic batholith, located in the Nanling Mountains of southern China. It is currently China's largest granite-associated uranium deposit, characterized as a typical thermal continental anomaly and a Mesozoic huge uranium-rich granite region (Zhong et al., 2023a, b). Hot springs in this region are commonly spatially associated with its numerous hydrothermal uranium deposits, as both are governed by the same underlying tectonic structures (Li et al., 2020). Several conceptual models have been proposed to explain uranium enrichment mechanisms, including supergene (Bonnetti et al., 2018), mantle-fluid (Shen et al., 2010), mantle-derived mineralizer (Hu et al., 2008; Zhang et al., 2017; Zhang et al., 2022), and basin-related models (Zhang et al., 2019; Chi et al., 2020). However, the relationship between geothermal anomalies and the radiogenic heat of uranium-rich granites in this region has received limited attention. In contrast to previous studies that primarily focus on uranium mineralization or mantle-derived heat flow, this study emphasizes the significant role of radiogenic heat production from uranium-rich granites in governing geothermal resource development within the Mianhuakeng uranium deposit (Zhou et al., 2000; Zheng et al., 2021; Li et al., 2023; Yuan et al., 2025).

This study systematically investigates the genesis mechanism of heat sources associated with geothermal resources in the Mianhuakeng deposit. By conducting rock thermophysical analyses, measuring radioactive heat production, and constructing a lithospheric thermal structure model, a theoretical foundation for the

development and utilization of uranium-thermal resources is established.

2 Geological Setting

The Mianhuakeng uranium deposit is located at the southeastern margin of the Zhuguangshan composite pluton, within the central segment of the Nanling Mountains, China (Fig. 1a). This region is situated in the subduction zone of the Pacific Plate along the southeastern margin of the Eurasian Continent. Regionally, the deposit is located within the NE-trending Wuyi–Yunkai arc–basin system. Its structural framework is influenced by several major uplift belts: the E–W trending Jiufeng–Dayu belt, the N–S trending Wanyang–Zhuguang belt, and the NE-trending Wanchangshan belt (Xu et al., 2012; Zhou et al., 2020; Wang et al., 2024).

The tectonic fabric in the study area is predominantly oriented northeast (Fig. 1b). Geological features found include the NNE-trending Tangdong fault, the NEE-trending Lizhou fault, the Mianhuakeng fault, the NWW-trending Youdong fault, and sub-NS-trending cleavage zones (Hu et al., 2008; Zhang et al., 2022). Among them, the Mianhuakeng fault and Youdong fault are the dominant structures in the study area, controlling the exposure and distribution of geothermal water (Zhong et al., 2023a). The Mianhuakeng fault is a post-mineralization, brittle compressional-shear structure, characterized by uncemented tectonic breccia consisting of rounded granite clasts and fault gouge. Cataclastic granite, a locally developed silicification zone, and ensuing white quartz veins identify the fault zone. The surrounding NEE

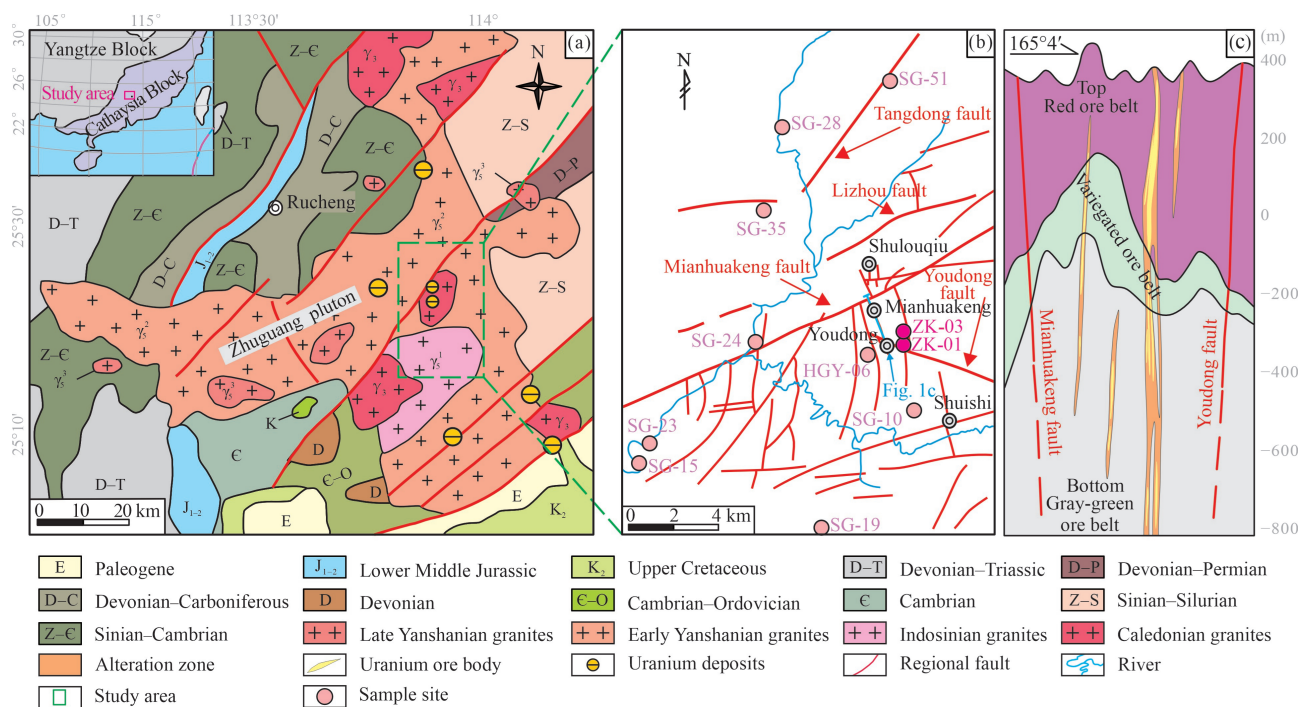


Fig. 1. Geological setting and sampling location of the study area.

(a) The locations of Cathaysian Block and Zhuguang pluton; (b) structural information and sample location of the study area; (c) hydrothermal alteration vertical zoning (modified after Qi et al., 2019; Chen C X et al., 2022; Zhang et al., 2022; Li et al., 2023 and Zhong et al., 2023b).

compressive stress field has an impact on the secondary cracks next to the fault, which primarily show NNW orientation (subparallel to NS). These formations are closely associated with uranium mineralization, despite having formed about 90 Ma later (Zhang et al., 2022; Zhong et al., 2023b). The Youdong fault is a SE-trending extensional-shear fracture zone. It is partially infilled by basic dykes dated about 110.6 ± 2.0 Ma and is characterized by a predominance of brittle fractures. Inside the fault zone are schistose basic dykes and cataclastic granites, as well as sporadic cases of "pig-liver" silicification linked to uranium mineralization (Zhang et al., 2007; Chen B L et al., 2022).

The Mianhuakeng deposit is the largest granite-hosted hydrothermal-vein-type uranium deposit, with mineralization found in Triassic biotite granite (~226 Ma) and Jurassic two-mica granite (~160 Ma) (Zhang et al., 2017, 2018). Whole-rock geochemical data indicate that both granites are S-type, derived from the partial melting of Paleoproterozoic sedimentary rocks (Zhang et al., 2017, 2018; Zhong et al., 2023b). In hydrothermal alteration zones, ore bodies typically occur as veins or lenses. The vertical depth of mineralization is more than 1000 meters (Zhong et al., 2019). Pitchblende is the primary ore material, occurring in a microcrystalline quartz vein with hematite and pyrite. U-Pb and Sm-Nd dating indicate a pitchblende age of approximately 70 Ma (Huang et al., 2010; Zhong et al., 2019; Zhang et al., 2022).

Subduction of the Pacific Plate caused asthenospheric upwelling (Fig. 1c), creating a high regional heat flow background (Pollack et al., 1993; Jiang et al., 2016). Drilling data obtained from depths of 150 to 1200 m reveal an average heat flow of 71.47 mW/m². This value exceeds the continental average for mainland China (Table 1; Jiang et al., 2016). Furthermore, the lithosphere in this area has a "hot crust" thermal structure, in which crustal heat flow constitutes the primary component of the total surface heat flow (Zheng and Luo, 2024). The largest energy source in the crust is the heat generated by radioactive decay. Granites in the Mianhuakeng uranium deposit, particularly the uranium-rich varieties, significantly influence the distribution and formation of geothermal resources through their elevated radiogenic heat production (Zhou et al., 2020).

3 Data and Methods

3.1 Sample collection and testing

The 30 sets of samples (mainly to measure thermal conductivity), and 15 sets of whole rock analysis samples (primarily for evaluating radiogenic heat production), were obtained from two boreholes and a 100 km² area of the Mianhuakeng uranium deposit's surface (Table 2). All samples were collected in a dried condition. Both surface and borehole samples were massive, predominantly comprising granite, quartzite (including veins), and metamorphic rocks. Bulk density was determined using a buoyancy method densitometer with an electronic balance (precision: 0.01 g). The TCS (Thermal Conductivity Scanning) automatic scanner is used to measure the thermal conductivity of rocks. With a range of 0.2 to 25 W/m·K, the measurement accuracy is $\pm 3\%$. A planar thin film thermal analyzer (thickness 0.2 mm, voltage 1.5–2.0 V) employing the unsteady heat transfer method was utilized to assess thermal conductivity. Standard reference materials (stainless steel and crystalline silica glass) were used for calibration. Their certified thermal conductivities at ambient temperature are 14.52 W/(m·K) and 1.15 W/(m·K), respectively. Whole-rock analysis includes the measurement of radioactive element U, Th and K content. First, whole-rock samples were made into a dry powder state, and the U and Th contents were determined by plasma mass spectrometer (ICP-MS). The content of K is generally expressed by the content of oxide K₂O, which is measured by wavelength dispersive X-ray fluorescence spectrometer. All chemical analyses were performed by Langfang Zhongtie Geophysical Prospecting Co., Ltd.

3.2 Calculation of radiogenic heat production of rocks

The density and the concentration of radiogenic heat-production elements (U, Th, and K) in rock are directly connected with the radiogenic heat production of the rock. Several equations have been established to calculate radiogenic heat production (Rybach, 1976; Wollenberg and Smith, 1987), Rybach's method remains the most widely adopted. The calculating formula is as follows (Rybach, 1976):

$$A = 0.01\rho(9.52C_U + 2.56C_{Th} + 3.48C_K) \quad (1)$$

Table 1 Existing terrestrial heat flow data in the surrounding counties of the Mianhuakeng uranium deposit (Xiong et al., 1993)

Location	NO.	Depth (m)	Measured heat flow	Correct heat flow
			($\mu\text{W}/\text{m}^2$)	($\mu\text{W}/\text{m}^2$)
Renhua County, Shaoguan City, Guangdong Province	1	80–150	65.9	65.9
	2	220–280	74.8	74.8
	3	210–300	76.9	76.9
	4	215–1200	90.4	88.7
Lechang City, Shaoguan City, Guangdong Province	5	280–480	71.7	71.7
	6	360–460	62.7	62.7
Nanxiong City, Shaoguan City, Guangdong Province	7	180–510	62.7	62.7
	8	370–500	65.8	65.8
	9	220–580	67.1	67.1
Chongyi County, Ganzhou City, Jiangxi Province	10	380–450	69.9	78.4

Table 2 The results of thermal properties and radiogenic heat production of samples

Sample No.	Type	Lithology	Depth (m)	Thermal conductivity (W/(m·K))	C_{Th} (ppm)	C_U (ppm)	C_K (wt%)	ρ (g/cm ³)	A (μ W/m ³)
SG-15	Outcrop	Quartz vein	0	5.81	0.048	0.051	0.131	2.6	0.03
SG-19	Outcrop	Granite	0	2.01	—	—	—	—	—
HGY-06	Outcrop	Granite	0	2.79	32.3	14.2	5.14	2.526	5.96
SG-10	Outcrop	Granite	0	2.99	—	—	—	—	—
SG-23	Outcrop	Metamorphic sandstone	0	3.36	14.1	2.84	3.21	2.65	1.97
SG-24	Outcrop	Alkali metasomatic rock	0	1.48	—	—	—	—	—
SG-28	Outcrop	Alkali metasomatic rock	0	2.92	—	—	—	—	—
SG-35	Outcrop	Altered cataclastic granite	0	3.07	20.3	20	5.32	2.537	6.62
SG-51	Outcrop	Mylonite	0	2.95	16.8	4.42	2.59	2.52	2.37
ZK01-40	Drill core	Medium-grained biotite granite	−190	2.44	—	—	—	—	—
ZK01-80	Drill core	Altered cataclastic granite	−230	2.61	19.6	6.38	5.73	2.595	3.4
ZK01-120	Drill core	Medium-grained biotite granite	−270	3.67	—	—	—	—	—
ZK01-160	Drill core	Medium-grained biotite granite	−310	2.71	57.8	13.04	4.93	2.594	7.5
ZK01-200	Drill core	Medium-grained biotite granite	−350	2.25	—	—	—	—	—
ZK01-220	Drill core	Altered cataclastic granite	−370	6.3	19	30.39	1.22	2.568	8.79
ZK01-240	Drill core	Altered cataclastic granite	−390	4.43	—	—	—	—	—
ZK01-260	Drill core	Medium-grained biotite granite	−410	2.47	25	15.3	7.46	2.548	6
ZK01-280	Drill core	Medium-grained biotite granite	−430	2.76	—	—	—	—	—
ZK01-300	Drill core	Medium-grained biotite granite	−450	3.1	20.8	7.25	5.5	2.538	3.59
ZK03-20	Drill core	Medium-grained biotite granite	−170	2.64	32.1	13.9	6.15	2.563	6.05
ZK03-60	Drill core	Medium-grained biotite granite	−210	3.09	—	—	—	—	—
ZK03-96	Drill core	Medium-grained biotite granite	−246	3.27	34.3	13.9	4.34	2.569	6.04
ZK03-140	Drill core	Quartz vein	−290	5.62	—	—	—	—	—
ZK03-183	Drill core	Medium-grained biotite granite	−333	4.35	17.2	5.93	3.39	2.608	2.93
ZK03-207	Drill core	Medium-grained biotite granite	−357	2.55	—	—	—	—	—
ZK03-220	Drill core	Medium-grained biotite granite	−370	2.92	—	—	—	—	—
ZK03-241	Drill core	Altered cataclastic granite	−391	2.73	26.7	9.89	5.42	2.525	4.58
ZK03-259	Drill core	Altered cataclastic granite	−409	2.91	—	—	—	—	—
ZK03-282	Drill core	Medium-grained biotite granite	−432	3.18	—	—	—	—	—
ZK03-298	Drill core	Medium-grained biotite granite	−448	3.16	30	9	5.1	2.546	4.59

“—” represents unmeasured; A is the radiogenic heat production of the rock; ρ is the density of the rock; C_U , C_{Th} , and C_K are the contents of uranium, thorium, and potassium in the rock, respectively.

where A represents the rock's radiogenic heat production (μ W/m³), ρ represents the rock density (g/cm³), and C_U , C_{Th} , and C_K represent the concentrations of U (ppm), Th (ppm), and K (wt%) in the rock, respectively. Table 2 presents the results of the thermal physical property test and the calculations of radiogenic heat production.

4 Results

4.1 Thermal conductivity of rocks

The thermal conductivity of rock samples in the study area, as indicated in Table 2, ranges from 1.48 to 6.3 W/(m·K), with a mean value of 3.2 W/(m·K). The thermal conductivity of drill samples ranges from 2.25 to 6.3 W/(m·K), with a mean value of 3.29 W/(m·K). This value is slightly higher than that of outcrop samples at 3.04 W/(m·K). The difference is attributed to increased porosity from surface weathering, which reduces thermal conductivity. Given that the thermal conductivity of the surface pluton is comparatively reduced due to weathering, the unweathered borehole core more accurately reflects the local thermal conductivity characteristics. In this study, the average thermal conductivity of borehole samples is established at 3.29 W/(m·K), aligning with the classical thermal conductivity value of 3.15 ± 0.32 W/(m·K) for granite in southeastern China (Artemieva et al., 2017; Kuang et al., 2020).

4.2 Radiogenic heat production of rocks

Radiogenic heat production (A) quantifies the intrinsic

heat-generating capacity of rocks. It is a key parameter for analyzing lithospheric thermal structure, sedimentary basin evolution, and deep heat flow calculations (Robert, 1982; Kuang et al., 2020). With a mean of 4.69 μ W/m³, the evaluated radiogenic heat production of rocks in the study area ranges from 0.03 to 8.79 μ W/m³, which is much higher than the global average of 2.1 to 2.5 μ W/m³ (Wollenberg and Smith, 1987; Artemieva et al., 2017; Wang et al., 2023a). The radiogenic heat production of granite ranges from 2.93 to 8.79 μ W/m³, with an average of 5.50 μ W/m³, categorizing it as high-heat-producing granite (>5 μ W/m³; Kromkhun, 2010).

4.3 Th/U ratio of radioactive thermogenic rocks

In order to deepen the understanding of the role of these elements in the radiogenic heat generated from rocks, we may compute the Th/U ratio and the contribution rates of U and Th to K using the formula mentioned previously, specifically A_{Th}/A_K and A_U/A_K (Rybach, 1976). Table 3 shows that the Th/U ratio ranges from 0.63 to 4.96, with a mean of 2.62. Sample ZK01-220 exhibits the lowest Th/U ratio (0.63), indicating a significant uranium enrichment. Based on their Th/U ratio, the granite is divided into three categories: low uranium granite ($Th/U > 6$), normal granite ($3 < Th/U < 6$), and uranium-rich granite ($Th/U < 3$) (Xu et al., 1995). Therefore the samples from the Mianhuakeng uranium deposit are theoretically classified as uranium-rich, high-heat-producing granite.

Table 3 Thermal contribution and Th/U ratio of radioactive heating elements

Sample No.	Th/U	A_{Th} A_U A_K ($\mu\text{W}/\text{m}^3$)			A_{Th}/A_K	A_U/A_K
		A_{Th}	A_U	A_K		
HGY-06	2.27	2.09	3.41	0.45	4.62	7.56
SG-15	0.94	0	0.01	0.01	0.27	1.07
SG-23	4.96	0.96	0.72	0.3	3.23	2.42
SG-35	1.02	1.32	4.83	0.47	2.81	10.28
SG-51	3.8	1.08	1.06	0.23	4.77	4.67
ZK01-80	3.07	1.3	1.58	0.52	2.52	3.05
ZK01-160	4.43	3.84	3.22	0.45	8.62	7.24
ZK01-220	0.63	1.25	7.43	0.11	11.46	68.14
ZK01-260	1.63	1.63	3.71	0.66	2.47	5.61
ZK01-300	2.87	1.35	1.75	0.49	2.78	3.61
ZK03-20	2.31	2.11	3.39	0.55	3.84	6.18
ZK03-96	2.47	2.26	3.4	0.39	5.81	8.76
ZK03-183	2.9	1.15	1.47	0.31	3.73	4.79
ZK03-241	2.7	1.73	2.38	0.48	3.62	4.99
ZK03-298	3.33	1.96	2.18	0.45	4.33	4.83

$\text{Th}/\text{U} = C_{\text{Th}}/C_{\text{U}}$, $A_{\text{Th}} = 0.01\rho \cdot 2.56C_{\text{Th}}$, $A_{\text{U}} = 0.01\rho \cdot 9.52C_{\text{U}}$ and $A_{\text{K}} = 0.01\rho \cdot 3.48C_{\text{K}}$.

5 Discussion

5.1 Revelation of thermal conductivity of rocks

The high thermal conductivity of the quartz veins, ranging from 5.62 to 5.81 $\text{W}/(\text{m}\cdot\text{K})$ (Table 2; Fig. 2), is attributed to their high quartz content. Altered cataclastic granite shows a wide range of thermal conductivity, from 2.61 to 6.3 $\text{W}/(\text{m}\cdot\text{K})$. Localized anomalies in thermal conductivity are likely caused by hydrothermal siliceous infillings within fractures. In contrast, alkali metasomatic rocks have the lowest conductivity, ranging from 1.48 to 2.92 $\text{W}/(\text{m}\cdot\text{K})$. This low conductivity is attributed to their loose mineral fabric and high porosity. These results indicate that quartz enrichment improves thermal conductivity, while siliceous filling enhances heat transfer.

According to the vertical distribution of boreholes (Fig. 3a), the average thermal conductivity in the middle to deep layers (-200 to -400 m, 3.24 $\text{W}/(\text{m}\cdot\text{K})$) is higher than in the shallow layer (<-200 m, 2.82 $\text{W}/(\text{m}\cdot\text{K})$) due to increased hydrothermal activity and fracture siliceous filling. The thermal conductivity of altered cataclastic granite ZK01-220 (-370 m) and quartz vein ZK03-140 (-290 m) is elevated, potentially indicating the presence of hydrothermal channels. Moreover, the thermal conductivity of the bedrock at ZK01-220 (-370 m) and ZK03-140 exhibited a noticeable rise. In borehole ZK01, the thermal conductivity of the ZK01-240 sample reaches 4.43 $\text{W}/(\text{m}\cdot\text{K})$, thereafter decreasing to around 2.78 $\text{W}/(\text{m}\cdot\text{K})$. Similarly, in borehole ZK03, the thermal conductivity of the ZK03-183 sample reaches 4.35 $\text{W}/(\text{m}\cdot\text{K})$, thereafter decreasing to around 2.91 $\text{W}/(\text{m}\cdot\text{K})$. Therefore, localized enhancements in the thermal conductivity are attributed to the upward migration of siliceous hydrothermal fluids from deeper strata within the Mianhuakeng uranium deposit.

5.2 Insights from radiogenic heat production in rocks

The continental crust generates approximately one-third of the Earth's total radioactive heat through the decay of U, Th, and K, which collectively account for $\sim 99\%$ of the

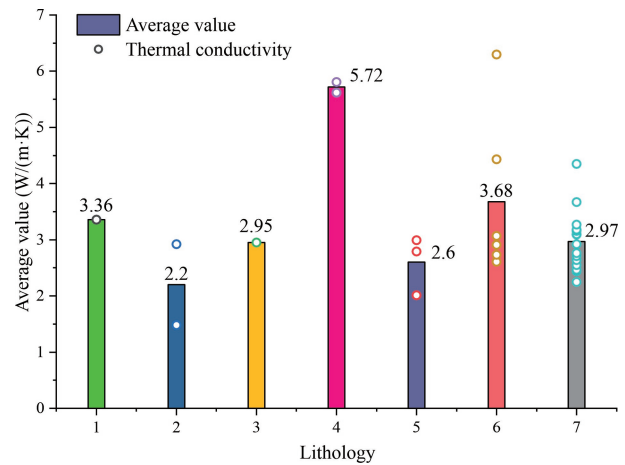


Fig. 2. Thermal conductivity distribution diagram of various lithology samples in the Mianhuakeng uranium deposit.

1: Metamorphic sandstone; 2: alkali metasomatic rock; 3: mylonite; 4: quartz vein; 5: granite; 6: altered cataclastic granite; 7: medium-grained biotite granite.

global radiogenic heat budget (Huang et al., 2013). Granite is a typical felsic rock with high levels of radioactive elements (U, Th, and K). As a major constituent of the upper crust, granite is also a significant source of radiogenically derived surface heat flow (Zhang et al., 2020).

The majority of the samples exhibit $A_{\text{Th}}/A_{\text{K}} < A_{\text{U}}/A_{\text{K}}$ (Table 3). This relationship indicates that U contributes more to the total radiogenic heat production than Th, consistent with the generally higher U concentrations measured in these rocks. Moreover, the study area is underlain predominantly by S-type granite, a rock type typically enriched in U. Over geological time, the abundances of both U and Th decrease. However, due to its shorter half-life, U decays faster than Th and therefore contributes more significantly to contemporary radiogenic heat production (Bea, 2012). Therefore, the uranium-rich and high-heat-producing granite in the study area serves as a significant heat source for the region.

Radiogenic heat production is typically highest in acidic rocks and limited in ultrabasic rocks. In borehole ZK01 (Fig. 3b), radiogenic heat production ranges from 3.39 to 8.79 $\mu\text{W}/\text{m}^3$, with a mean value of 5.12 $\mu\text{W}/\text{m}^3$. Shallow altered cataclastic granite exhibits 3.39 $\mu\text{W}/\text{m}^3$ of radiogenic heat, whereas medium-deep medium-grained biotite granite produces 7.50 $\mu\text{W}/\text{m}^3$. At -370 m, the altered cataclastic granite reaches a maximum of 8.79 $\mu\text{W}/\text{m}^3$, although the deeper layer exhibits notable fluctuations, dropping to 3.59 $\mu\text{W}/\text{m}^3$. At depths of -170 to -448 m, borehole ZK03 produces radiogenic heat at a mean of 4.83 $\mu\text{W}/\text{m}^3$, with a range of 2.93 to 6.05 $\mu\text{W}/\text{m}^3$. Shallow medium-grained biotite granite exhibits high values (6.04–6.05 $\mu\text{W}/\text{m}^3$). Values decrease to 2.93–4.58 $\mu\text{W}/\text{m}^3$ in medium-depth, unaltered granite, followed by a slight increase to 4.59 $\mu\text{W}/\text{m}^3$ in deeper sections (Fig. 3b). This vertical pattern suggests that the radiogenic heat production of granite in the Mianhuakeng area is strongly influenced by hydrothermal alteration.

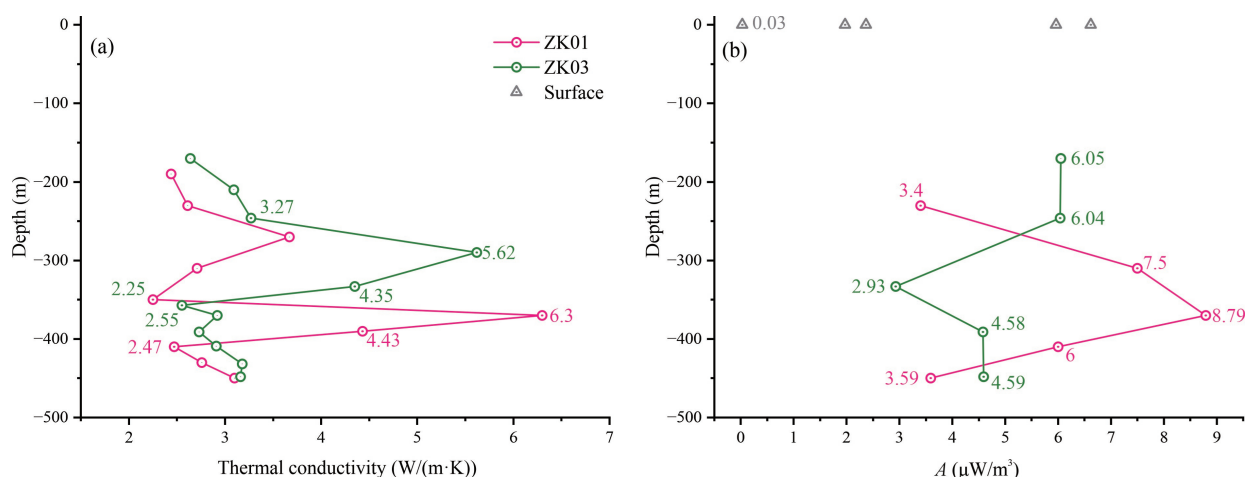


Fig. 3. The variation of thermal conductivity and radioactive heat production with depth of ZK01 and ZK03. (a) The variation of thermal conductivity with depth; (b) the relationship between radiogenic heat production and depth.

The radiogenic heat production of ZK01-220 sample is the highest ($8.79 \mu\text{W}/\text{m}^3$), which is altered cataclastic granite. These alteration processes resulted in widespread chloritization of the local rock (Wu et al., 2019). Clay minerals formed during alteration, such as chlorite, are effective scavengers of U and Th (Porcelli and Swarzenski, 2003; Manikyamba et al., 2018). The high radiogenic heat production of ZK01-220 sample may be related to the adsorption and enrichment of heat-producing elements by clay minerals in the later alteration process. During the alteration process, the formation of clay minerals such as chlorite increases the adsorption capacity of U and Th, thus enriching the radioactive elements in these minerals. This enrichment effect may lead to a higher radiogenic heat production of ZK01-220 samples than other samples. As a result, the uranium-rich ore body, its alteration halo, and the surrounding granitic host rock collectively constitute significant heat-generating bodies. Their combined radiogenic heat production is a major contributor to the crustal heat budget and plays a crucial role in shaping and sustaining the local thermal structure.

5.3 Thermal structure and thermal contribution characteristics

To address gaps in the existing database for radiogenic heat production of deep-seated plutons, we conducted a comprehensive review and synthesis of relevant literature. This approach ensured the accuracy and reliability of our findings. After collating and analyzing the gathered data, we find that the average radiogenic heat production of the granitic bedrock at depths of 0 to 5 km is $5.18 \mu\text{W}/\text{m}^3$ (Lin et al., 2017). According to statistical data, Wang et al. (2023b) determined that the average radiogenic heat productions of the top, middle, and lower crust in China's land area are $1.31 \mu\text{W}/\text{m}^3$, $0.57 \mu\text{W}/\text{m}^3$, and $0.22 \mu\text{W}/\text{m}^3$, respectively. Moreover, the temperature data from representative geothermal wells in surrounding areas (Fig. 4) indicate that the geothermal gradient of the shallow crust (<5 km) in the area remains relatively constant (Li et al., 2021). Therefore, these parameters provide the necessary constraints to model the regional lithospheric

thermal structure.

The terrestrial heat flow (q_0) measured at the surface consists of two components: the heat produced by the radioactive decay of isotopes U, Th, and K in the crust, known as crustal heat flow (q_c), and the heat originating from the mantle, referred to as mantle heat flow (q_m). Heat flow from the mantle is an important deep geophysical characteristic. Compared to surface heat flow, a key advantage of mantle heat flow is that it minimizes the influence of variable shallow crustal geology and near-surface environmental conditions. This provides a more robust signal for interpreting deep thermal processes (Li et al., 2017; Sun et al., 2021; Zhu et al., 2024; Wang et al.,

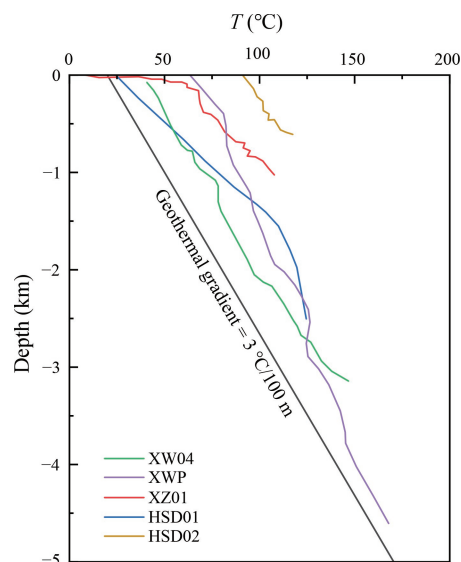


Fig. 4. Representative borehole temperature measurement curves in the surrounding counties of the Mianhuakeng uranium deposit (modified from Li et al., 2021). XW04 represents petroleum well in Leizhou Peninsula, XWP represents bottom temperature of petroleum well measurement in Leizhou Peninsular, XZ01, HSD01 and HSD02 represent geothermal energy scientific exploration wells in Huangshadong and Xinzhou area, and black line represents global average geothermal gradient line.

2025). The method for calculating mantle heat flow is based on a specified layered crustal model, utilizing the "stripping method" to identify the heat flow generated by the decay of radioactive elements in each structural layer. For each layer, the product of its thickness and average radiogenic heat production yields its heat flow contribution. The mantle heat flow (q_m) is then obtained by subtracting the summed crustal contributions from the total surface heat flow (q_0), which also defines the crust-to-mantle heat flow ratio. The relevant calculation formulas are as follows (Lachenbruch, 1968; Roy et al., 1968):

$$q_i = D_i \cdot A_i \quad (2)$$

$$q_c = \sum q_i \quad (3)$$

$$q_m = q_0 - q_c \quad (4)$$

where D_i represents the thickness of the structural layer, A_i represents the associated radiogenic heat production of the layer, while q_i , q_c , and q_m represent the heat flow values generated by the radioactive decay of each structural layer, the radioactive elements within all crustal strata, and the mantle heat flow value, respectively. The ratio of crust-mantle heat flow distribution is q_c/q_m , and the total surface heat flow value is the regional average of 57.16 mW/m² (Table 4, the geothermal gradient fitted according to the least-square method). According to the Crust1.0 model (Laske et al., 2013), the lithospheric structure of the Mianhuakeng deposit has been classified (Table 5): the granite-dominated bedrock layer has a thickness of 5 km, the upper crust is around 6 km, the middle crust is about 11 km thick, and the lower crust also has a thickness of about 11 km (Pasyanos et al., 2014).

Table 5 presents the outcomes of incorporating the average heat flow value, layer thickness, and radiogenic heat production statistics for each crustal segment into formulas 2, 3, and 4. The heat flow value generated by the decay of radioactive elements in rocks, from the surface to the Moho layer, is 42.45 mW/m² for crustal heat flow, 14.71 mW/m² for mantle heat flow, and the ratio of crustal to mantle heat flow in the area is 2.89, indicating a major

contribution of crustal heat to the heat source. Analysis result shows that the near-surface granite layer exhibits the highest radiogenic heat production. Although it is the thinnest layer, it contributes approximately 45% of the total crustal radiogenic heat, significantly exceeding the mantle-derived heat contribution (~26.3%). The total heat flow generated by the upper crust and the granite layer is 33.76 mW/m², with a contribution rate of approximately 58.6% (>50%). This result demonstrates that radiogenic heat from the upper crust, particularly the granite layer, is a major source for the regional geothermal resources.

5.4 Genetic model of heat source of Mianhuakeng uranium deposit

Meteoric water is the source for the initial hydrothermal fluid. This fluid undergoes deep circulation within the fault zone, where it mixes with carbon dioxide derived from the deep mantle. The resulting mixed fluid then circulates through the host granite, leaching uranium (U) and other metals (e.g., Fe, Th) to form a mineralizing fluid (Hu et al., 2008; Ling, 2011; Zhang et al., 2022). Pre-ore hydrothermal alteration enhances fluid circulation efficiency and improves U leaching rates. Uranium in granite releases mobile UO₂²⁺ through hydrothermal alteration, acting as the primary source for mineralization. The Mianhuakeng and Youdong faults serve as primary conduits for the vertical migration of ore-forming thermal fluids, enabling the movement of hydrothermal fluids from depths exceeding 5 km to shallower regions. As these fluids ascend, decreasing temperature, pressure, and oxygen fugacity trigger CO₂ degassing, which lowers the fluid pH. Then Fe²⁺ from the rebalancing of iron-rich and magnesium-rich conditions reduced free U⁶⁺ to U⁴⁺ and precipitated as pitchblende, resulting in the formation of uranium deposits (UO₂) in the shallow granite (Hu et al., 2008; Zhang et al., 2022; Zhong et al., 2023b). The uranium-rich granite formation and associated alteration zone provide a stable and high-heat-producing body. This radiogenic heat continuously drives hydrothermal circulation, in which heated fluids rise along fault

Table 4 Geothermal gradient and terrestrial heat flow calculation results table of borehole test section

Drilling No.	Heat flow calculation section (m)	Linear regression equation and correlation coefficient R^2 (least-square method)	Geothermal gradient (°C/km)	Average thermal conductivity of rock (W/(m·K))	Heat flow (mW/m ²)
ZK01	170–300	$y = -17.9x + 34.8$ $R^2 = 0.983$	17.9	2.91	52.10
ZK03	170–300	$y = -17.0x + 39.7$ $R^2 = 0.977$	17.0	3.66	62.22

Table 5 Calculation results of lithospheric thermal structure in Mianhuakeng uranium deposit

Structural layer	Elevation (km)	Depth (km)	Calculate layer segments (km)	A_i (μW/m ³)	D_i (km)	q_i (mW/m ²)	Top heat flow(mW/m ²)	Thermal contribution rate (%)
Earth's surface	0.25	0	—	—	—	—	—	—
Granite	-4.75	5	0–5	5.18	5	25.9	57.16	44.97
Upper crust	-10.75	11	6–11	1.31	6	7.86	31.26	13.65
Middle crust	-21.75	22	11–22	0.57	11	6.27	23.4	10.89
Lower crust	-32.75	33	22–33	0.22	11	2.42	17.13	4.20
Outer mantle	—	—	—	—	—	—	14.71	26.29

D_i is the thickness of the structural layer; A_i is the corresponding radiogenic heat production of the layer; and q_i is the heat flow value generated by the radioactive decay of each layer of rock.

fractures and mix with shallow, cooler groundwater, to form the shallow geothermal water observed today.

The genetic model of this uranium-thermal symbiotic resource is illustrated in Fig. 5. Subduction of the Pacific Plate induces a substantial temperature anomaly at the plate's leading edge, resulting in an uplift of the asthenosphere and the rise of thermal material along deep NE-trending regional faults into the middle and upper crust. These mantle-derived thermal material (including

volatile components such as U) ascend along Mianhuakeng and Youdong fault cracks, forming a relatively high mantle-derived heat source. In addition, uranium-rich granite in the crust provides a major crustal heat source, contributing approximately 45% of the total thermal budget through its elevated radiogenic heat production. Together, the mantle-derived heat flow and the crustal radiogenic heat form an integrated heat source system. Major faults serve as conduits for the vertical

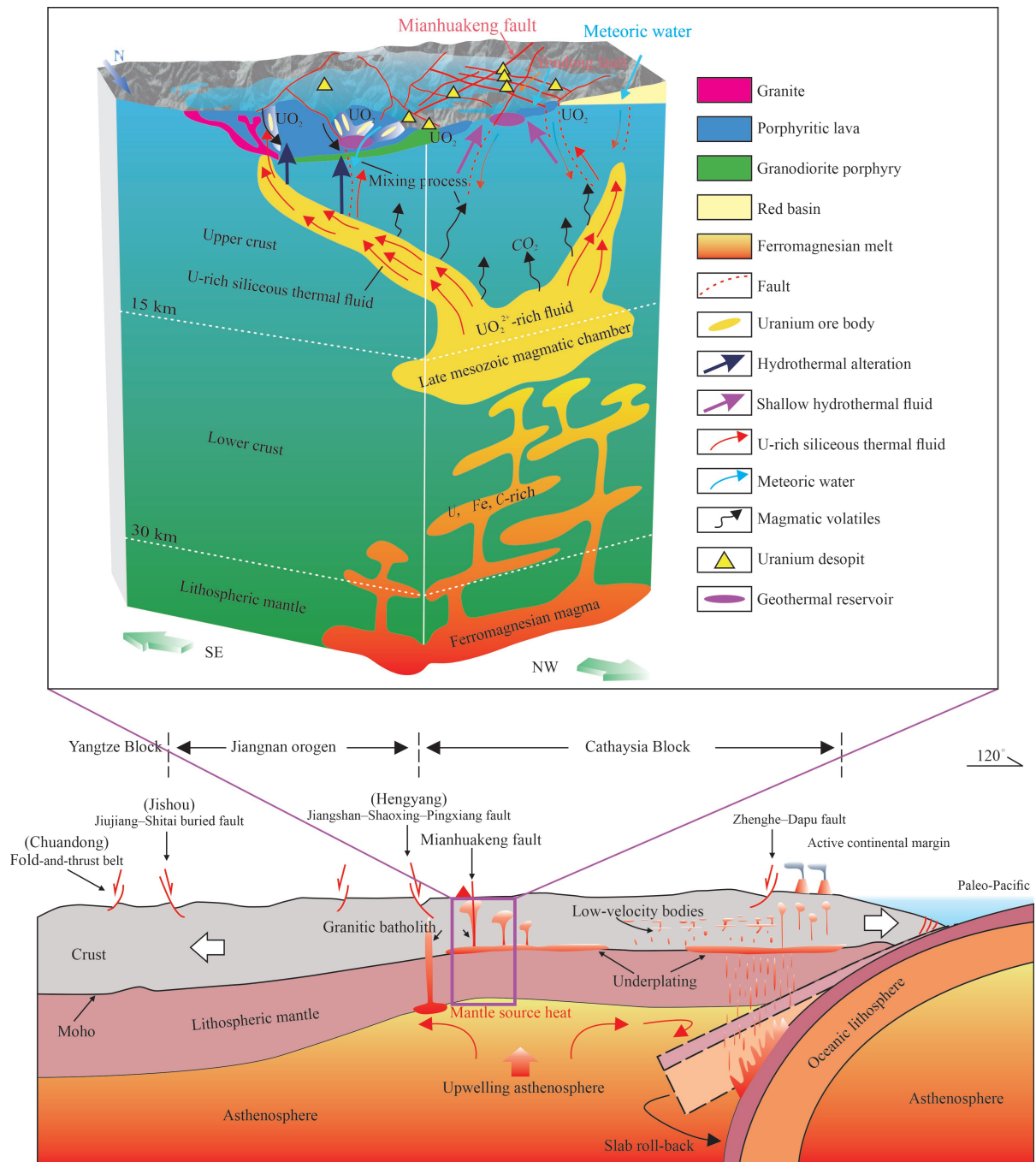


Fig. 5. The conceptual model of the heat source genesis mechanism of the Mianhuakeng uranium deposit (modified after Chen C X et al., 2022 and Li et al., 2023).

migration and lateral redistribution of both heat and uranium-bearing ore-forming fluids, controlling their flow, focusing, and eventual deposition. Uranium enrichment not only further increases the granite's radiogenic heat production but also extends the thermal longevity of the geothermal system.

6 Conclusions

(1) The granite in Mianhuakeng uranium deposit is characterized by a high radioactive heating rate (avg. $5.50 \mu\text{W}/\text{m}^3$) and a low Th/U ratio (avg. 2.62), which belongs to the uranium-rich and high-heat-producing granite. Hydrothermal alteration enhances the thermal property of granite. Quartz enrichment increases thermal conductivity, while siliceous fracture fillings enhance localized heat transfer. Deep siliceous hydrothermal activity promotes the activation, migration, and adsorption of U, leading to its enrichment. Consequently, U contributes more to the total radiogenic heat production than Th or K.

(2) Crustal heat is a dominant component of the heat budget, as indicated by a crust-to-mantle heat flow ratio of 2.89. Especially in the shallow crust up to 5 km, the uranium-rich granite body and associated alteration zone constitute a stable and high-heat-producing source. This granitic complex contributes approximately 45% of the total heat.

(3) This study proposes a geological model for uranium-geothermal symbiosis at tectonic plate margin. The model comprises two key stages: First, the subduction of the Pacific Plate drove asthenospheric upwelling, with mantle-derived heat and material transferred to the mid-to-upper crust. Second, deep-seated faults (e.g., Mianhuakeng and Youdong faults) served as conduits for the vertical and lateral transport of both heat and uranium-mineralizing fluids, controlling their focusing and deposition, which leads to the formation of uranium-rich granite in the shallow crust. This mechanism provides a theoretical basis for the co-exploration and development of uranium-geothermal symbiotic resources in South China.

Acknowledgments

This study was financially supported by the National Natural Science Foundation of China (41902310, 42372348, 42372286), Deep Earth Probe and Mineral Resources Exploration—National Science and Technology Major Project (2024ZD1003607), China Geological Survey Projects (DD20230700802, DD20221819); the Basic Research Fund of the Chinese Academy of Geological Sciences (JKYQN202306) and Key Research and Development Program of Shanxi Province, China (202102090301009).

Manuscript received May 15, 2025
accepted Nov. 04, 2025
associate EIC: XU Tianfu
edited by GUO Xianqing

References

Abbady, A.G., and Al-Ghamdi, A., 2018. Heat production rate

- from radioactive elements of granite rocks in north and southeastern Arabian shield Kingdom of Saudi Arabia. *Journal of Radiation Research Applied Sciences*, 11(4): 281–290.
- Artemieva, I.M., Thybo, H., Jakobsen, K., Sørensen, N.K., and Nielsen, L.S.K., 2017. Heat production in granitic rocks: Global analysis based on a new data compilation GRANITE2017. *Earth Science Reviews*, 172: 1–26.
- Bea, F., 2012. The sources of energy for crustal melting and the geochemistry of heat-producing elements. *Lithos*, 153: 278–291.
- Bonnetti, C., Liu, X., Mercadier, J., Cuney, M., Deloule, E., Villeneuve, J., and Liu, W., 2018. The genesis of granite-related hydrothermal uranium deposits in the Xiashuang and Zhuguang ore fields, North Guangdong Province, SE China: Insights from mineralogical, trace elements and U-Pb isotopes signatures of the U mineralisation. *Ore Geology Reviews*, 92: 588–612.
- Chen, B.L., Gao, Y., Shen, J.H., and Zeng, G.Q., 2022. Characteristics of the Mianhuakeng fault and Youdong fault and their relation to uranium mineralization in the Changjiang uranium ore field, northern Guangdong. *Journal of Geomechanics*, 28(3): 367–382 (in Chinese with English abstract).
- Chen, C.X., Lü, Q.T., Chen, L., Shi, D.N., Yan, J.Y., and Ai, Y.S., 2022. Crustal thickness and composition in the South China Block: Constraints from earthquake receiver function. *Science China Earth Sciences*, 65(4): 698–713.
- Chi, G.X., Ashton, K., Deng, T., Xu, D.R., Li, Z.H., Song, H., Liang, R., and Kennicott, J., 2020. Comparison of granite-related uranium deposits in the Beaverlodge district (Canada) and South China—A common control of mineralization by coupled shallow and deep-seated geologic processes in an extensional setting. *Ore Geology Reviews*, 117: 103319.
- Erbek, E., and Dolmaz, M.N., 2019. Investigation of the thermal structure and radiogenic heat production through aeromagnetic data for the southeastern Aegean Sea and western part of Turkey. *Geothermics*, 81: 113–122.
- Furlong, K.P., and Chapman, D.S., 2013. Heat flow, heat generation, and the thermal state of the lithosphere. *Annual Review of Earth*, 41(1): 385–410.
- Hu, R.Z., Bi, X.W., Zhou, M.F., Peng, J.T., Su, W.C., Liu, S., and Qi, H.W., 2008. Uranium metallogenesis in South China and its relationship to crustal extension during the Cretaceous to Tertiary. *Economic Geology*, 103(3): 583–598.
- Huang, G.L., Yin, Z.P., Ling, H.F., Deng, P., Zhu, B., and Shen, W.Z., 2010. Formation age geochemical characteristics and genesis of pitchblende from No. 302 uranium deposit in Northern Guangdong. *Mineral Deposits*, 29: 352–360 (in Chinese with English abstract).
- Huang, Y., Chubakov, V., Mantovani, F., Rudnick, R.L., and McDonough, W.F., 2013. A reference Earth model for the heat-producing elements and associated geoneutrino flux. *Geochemistry, Geophysics, Geosystems*, 14(6): 2003–2029.
- Jiang, G.Z., Gao, P., Rao, S., Zhang, L.Y., Tang, X.Y., Huang, F., Zhao, P., Pang, Z.H., He, L.J., and Hu, S.B., 2016. Compilation of heat flow data in the continental area of China. *Chinese Journal of Geophysics*, 59(8): 2892–2910.
- Jiang, Z.J., Xu, T.F., Mallants, D., Tian, H.L., and Owen, D.D.R., 2019. Numerical modelling of stable isotope (^2H and ^{18}O) transport in a hydro-geothermal system: Model development and implementation to the Guide Basin, China. *Journal of Hydrology*, 569: 93–105.
- Kremenetsky, A., Milanovsky, S.Y., and Ovchinnikov, L., 1989. A heat generation model for continental crust based on deep drilling in the Baltic Shield. *Tectonophysics*, 159(3–4): 231–246.
- Kromkhun, K., 2010. Petrogenesis of high heat producing granite: Implication for Mt Painter Province, South Australia (Ph.D. thesis). Adelaide SA: University of Adelaide.
- Kuang, J., Qi, S.H., Wang, S., Xiao, Z.C., Zhang, M., Zhao, X., and Gan, H.N., 2020. Granite intrusion in Huizhou, Guangdong Province and its geothermal implications. *Earth Science*, 45(4): 1466–1480 (in Chinese with English abstract).
- Lachenbruch, A.H., 1968. Preliminary geothermal model of the Sierra Nevada. *Journal of Geophysical Research*, 73(22): 6977–

- 6989.
- Laske, G., Masters, G., Ma, Z.T., and Pasyanos, M., 2013. Update on CRUST1.0—A 1-degree global model of Earth's crust. *Geophysical research abstracts*, 15(15): 2658.
- Li, Y.M., Tian, J., Cheng, Y.Z., Jiang, G.Z., Zhang, Y., Chen, K., and Pang, Z.H., 2021. Existence of high temperature geothermal resources in the igneous rock regions of South China. *Frontiers in Earth Science*, 9: 728162.
- Li, Y.M., Luo, J., Tian, J., Cheng, Y.Z., Pang, Z.H., Huang, T.M., and Fan, Y.F., 2023. Formation of the hydrothermal system from granite reservoir for power generation in igneous rock areas of South China. *Geothermics*, 110: 102673.
- Li, Y.Y., Duo, J., Zhang, C.J., Chi, G.X., Wang, G.L., Zhang, F.F., Xing, Y.F., and Zhang, B.J., 2020. Genetic relationship between geothermal energy and hydrothermal uranium deposits: Research progress and method. *Geological Review*, 66(5): 1361–1375 (in Chinese with English abstract).
- Li, Z.X., Zuo, Y.H., Qiu, N.S., and Gao, J., 2017. Meso–Cenozoic lithospheric thermal structure in the Bohai Bay Basin, eastern North China Craton. *Geoscience Frontiers*, 8(5): 977–987.
- Lin, L.F., Sun, Z.X., Wang, A.D., Liu, J.H., Wan, J.J., Li, X.C., and Luo, X.W., 2017. Radioactive geochemical characteristics of Mesozoic granites from Nanling region and southeast coastal region and their constraints on lithospheric thermal structure. *Acta Petrologica et Mineralogica*, 36(4): 488–500 (in Chinese with English abstract).
- Ling, H.F., 2011. Origin of hydrothermal fluids of granite-type uranium deposits: Constraints from redox conditions. *Geological Review*, 57(2): 193–206 (in Chinese with English abstract).
- Manikyamba, C., Said, N., Santosh, M., Saha, A., Ganguly, S., and Subramanyam, K., 2018. U enrichment and Th/U fractionation in Archean boninites: Implications for paleo-ocean oxygenation and U cycling at juvenile subduction zones. *Journal of Asian Earth Sciences*, 157: 187–197.
- Mareschal, J.C., and Jaupart, C., 2013. Radiogenic heat production, thermal regime and evolution of continental crust. *Tectonophysics*, 609: 524–534.
- Pasyanos, M.E., Masters, T.G., Laske, G., and Ma, Z., 2014. LITHO1.0: An updated crust and lithospheric model of the Earth. *Journal of Geophysical Research: Solid Earth*, 119(3): 2153–2173.
- Pollack, H.N., Hurter, S.J., and Johnson, J.R., 1993. Heat flow from the Earth's interior: Analysis of the global data set. *Reviews of Geophysics*, 31(3): 267–280.
- Porcelli, D., and Swarzenski, P.W., 2003. The behavior of U- and Th-series nuclides in groundwater. *Reviews in Mineralogy Geochemistry*, 52(1): 317–361.
- Qi, J.M., Zhu, Z., Wu, J.Y., Cao, H.J., Liu, W.Q., and Xu, Z.Q., 2019. The evolution of ore-forming fluid and its constraint on mineralization process in Mianhuakeng uranium deposit, northern Guangdong, China. *Acta Petrologica Sinica*, 35(9): 2711–2726 (in Chinese with English abstract).
- Roy, R.F., Blackwell, D.D., and Birch, F., 1968. Heat generation of plutonic rocks and continental heat flow provinces. *Earth and Planetary Science Letters*, 5: 1–12.
- Rybach, L., 1976. Radioactive heat production in rocks and its relation to other petrophysical parameters. *Pure and Applied Geophysics*, (No. 2): 309–317.
- Shen, W.Z., Ling, H.F., Deng, P., Zhu, B., Huang, G.L., and Tan, Z.Z., 2010. Study on isotope geochemistry of uranium deposit 302 in northern Guangdong province. *Uranium Geology*, 26(2): 80–87 (in Chinese with English abstract).
- Sun, G.Z., Liu, S.W., Cawood, P.A., Tang, M., van Hunen, J., Gao, L., Hu, Y.L., and Hu, F.Y., 2021. Thermal state and evolving geodynamic regimes of the Meso- to Neoproterozoic North China Craton. *Nature Communications*, 12(1): 3888.
- Robert, S.C., 1982. *Handbook of Physical Properties of Rocks*. Boca Raton: CRC Press, 281–293.
- Wan, J.J., Sun, Z.X., Hu, B.Q., Wang, A.D., Liu, J.H., Liu, C.D., Chen, G.X., and Li, X.C., 2015. Radiogenic geochemistry investigation on granitic rocks from Fogang complex, northern Guangdong province and its implications for hot dry rock resource. *Journal of East China Institute of Technology* (Natural Science Edition), 38(4): 398–406 (in Chinese with English abstract).
- Wang, L.Y., Liu, K., Ma, Y., Zhang, Y.Y., Tong, J., Jia, W.H., Zhang, S.C., and Sun, J.L., 2024. Geochemical and isotopic techniques constraints on the origin, evolution, and residence time of low-enthalpy geothermal water in western Wugongshan, SE China. *Acta Geologica Sinica (English Edition)*, 98(3): 801–818.
- Wang, G.L., Gan, H.N., Lin, W.J., Yue, G.F., Yan, X.X., Li, T.X., Zhang, W., and Ma, F., 2023a. Hydrothermal systems characterized by crustal thermally-dominated structures of southeastern China. *Acta Geologica Sinica (English Edition)*, 97(4): 1003–1013.
- Wang, G.L., Liu, F., Lin, W.J., Zhang, W., Yuan, R.X., Xi, Y.F., Wei, S.C., Liao, Y.Z., and Wang, Y.R., 2023b. The crustal heat production rate and crustal and mantle heat flow distribution in the land areas of China. *Chinese Journal of Geophysics*, 66(12): 5041–5056 (in Chinese with English abstract).
- Wang, Y.B., Wang, Y.Q., Zhong, Z.N., Chen, C.Q., Guo, L.Y., Zhang, H.H., He, L.J., and Hu, S.B., 2025. Heat flow, lithospheric thermal structure, and its tectonic implication of the Southern North China Basin, East-central China. *Geothermics*, 130: 103336.
- Wollenberg, H., and Smith, A., 1987. Radiogenic heat production of crustal rocks: An assessment based on geochemical data. *Geophysical Research Letters*, 14(3): 295–298.
- Wu, D.H., Xia, F., Pan, J.Y., Liu, G.Q., Huang, G.L., Liu, W.Q., and Wu, J.Y., 2019. Characteristics of hydrothermal alteration and material migration of Mianhuakeng uranium deposit in northern Guangdong Province. *Acta Petrologica Sinica*, 35(9): 2745–2764 (in Chinese with English abstract).
- Xiong, L.P., Hu, S.B., and Wang, J.Y., 1993. Terrestrial heat flow values in southeastern China. *Chinese Journal of Geophysics*, 36(6): 784–790 (in Chinese with English abstract).
- Xu, B.L., Yan, G.H., Zhao, H., and Zhang, Z.L., 1995. Geochemistry of K₂O–U–Th elements of granites from Eastern China. *Acta Scientiarum Naturalium Universitatis Pekinensis*, 31(4): 444–450 (in Chinese with English abstract).
- Xu, Y.G., Wei, J.X., Qiu, H.N., Zhang, H.H., and Huang, X.L., 2012. Opening and evolution of the South China Sea constrained by studies on volcanic rocks: Preliminary results and a research design. *Chinese Science Bulletin*, 57: 3150–3164.
- Yang, L.Z., Liu, J.H., Sun, Z.X., Wang, A.D., Wan, J.J., and Zhou, Y., 2016. Study of the characteristics of radioactive heat production rate and hot dry rock resources potential in Zhangzhou city. *Modern Mining*, 32(3): 123–127, 133 (in Chinese with English abstract).
- Yang, Y.G., Tao, J.H., Xu, Z.T., Feng, Z.J., Sun, J.J., Ren, Z., Leng, C.B., and Tang, W.J., 2025. Geochemical characteristics of apatite in granites from Xiazhuang uranium ore field of northern Guangdong Province and their implications for petrogenesis and mineralization. *Acta Petrologica Sinica*, 41(9): 3019–3037 (in Chinese with English abstract).
- Yuan, Y.L., Zhang, X.L., Yu, H., Zhong, C.H., Wang, Y., Wen, D.G., Xu, T.F., and Gherardi, F., 2025. Research progress and technical challenges of geothermal energy development from hot dry rock: A review. *Energies*, 18(7): 1742.
- Zhang, C., Cai, Y.Q., Dong, Q., Xu, H., and He, S., 2019. Genesis of the South Zhuguang uranium ore field, South China: Fluid inclusion and H–C–O–S–Sr isotopic constraints. *Applied Geochemistry*, 100: 104–120.
- Zhang, C., Hu, S.B., Song, R.C., Zuo, Y.H., Jiang, G.Z., Lei, Y.D., Zhang, S.S., and Wang, Z.T., 2020. Genesis of the hot dry rock geothermal resources in the Gonghe basin: Constraints from the radiogenic heat production rate of rocks. *Chinese Journal of Geophysics*, 63(7): 2697–2709.
- Zhang, G.Q., Hu, R.Z., Shang, P.Q., Liu, L., and Yang, S.F., 2007. An overview on the ore-forming mechanism of the granite-type uranium deposit in South China. *Bulletin of Mineralogy, Petrology and Geochemistry*, 26(4): 399–404 (in Chinese with English abstract).
- Zhang, L., Chen, Z.Y., Li, S.R., Santosh, M., Huang, G.L., and Tian, Z.J., 2017. Isotope geochronology, geochemistry, and mineral chemistry of the U-bearing and barren granites from

- the Zhuguangshan complex, South China: Implications for petrogenesis and uranium mineralization. *Ore Geology Reviews*, 91: 1040–1065.
- Zhang, L., Chen, Z.Y., Li, S.R., Santosh, M., and Huang, G.L., 2018. Zircon U-Pb geochronology and geochemistry of granites in the Zhuguangshan complex, South China: Implications for uranium mineralization. *Lithos*, 308: 19–33.
- Zhang, Y.Y., Zhong, F.J., Liu, J.G., Qi, J.M., Pan, J.Y., Xia, F., and Li, H.D., 2022. Genesis of the Mianhuakeng uranium deposit, South China: Constraints from in-situ sulfur isotopes and trace elements of pyrite. *Applied Geochemistry*, 140: 105302.
- Zheng, H.R., and Luo, J., 2024. Progress in research on the exploration and evaluation of deep geothermal resources in the Fujian–Guangdong–Hainan region, China. *Energy Geoscience*, 5(2): 100232.
- Zheng, H.R., Luo, J., Zhang, Y., Feng, J.Y., Zeng, Y., and Wang, M.C., 2021. Geological characteristics and distribution of granite geothermal reservoir in southeast coastal areas in China. *Frontiers in Earth Science*, 9: 683696.
- Zhong, F.J., Pan, J.Y., Zhang, W.M., Lai, J., Zhou, T.B., and Liu, W.Q., 2019. Magmatism, tectonic activity and uranium mineralize events of Zhuguang south uranium ore-concentrated district, Northern Guangdong, China. *Journal of Geomechanics*, 25(S1), 108–114 (in Chinese with English abstract).
- Zhong, F.J., Wang, L., Wang, K.X., Liu, J.G., Zhang, Y., Li, H., Yang, S., Chen, Y.P., Xia, F., and Pan, J.Y., 2023a. Mineralogy and geochemistry of hydrothermal alteration of the Mianhuakeng uranium deposit in South China: Implications for mineralization and exploration. *Ore Geology Reviews*, 160: 105606.
- Zhong, F.J., Zhang, X.T., Wang, K.X., Wu, B., Liu, J.G., Pan, J.Y., and Xia, F., 2023b. Genesis of the Mianhuakeng granite-related uranium deposit, South China: Insights from cathodoluminescence imaging, fluid inclusions, and trace elements composition of hydrothermal quartz. *Ore Geology Reviews*, 154: 105308.
- Zhou, X.M., and Li, W.X., 2000. Origin of Late Mesozoic igneous rocks in Southeastern China: Implications for lithosphere subduction and underplating of mafic magmas. *Tectonophysics*, 326(3–4): 269–287.
- Zhou, Z.M., Ma, C.Q., Qi, S.H., Xi, Y.F., and Liu, W., 2020. Late Mesozoic high-heat-producing (HHP) and high-temperature geothermal reservoir granitoids: The most significant geothermal mechanism in South China. *Lithos*, 366: 105568.
- Zhu, W.J., and Liu, S.W., 2024. Heat flow and thermal structure of the South China Sea. *Earth Science Reviews*, 261: 105028.

About the first author

WANG Siqu, female, born in 1990 in Shijiazhuang, Hebei Province; Ph.D. graduated from China University of Geosciences (Beijing) in 2017; Senior engineer. She is now mainly engaged in hydrogeochemistry, geothermal genetic mechanisms, and geothermal resource exploration and utilization. E-mail: wsiqu17@163.com.

About the corresponding author

ZHANG Baojian, male, born in 1972 in Dezhou, Shandong Province; Ph.D. graduated from China University of Geosciences (Beijing) in 2011; Professor level senior engineer. He mainly engages in research on the genesis mechanism of geothermal resources and selection of target area, hydrogeological and environmental geology, carbon sequestration. E-mail: zbjsddk@126.com.